Turk J Phys
29 (2005) , 329 – 340.

Physical Properties of Holmium Promoted Superconductivity in Nd-Doped YBCO HT_C-Superconductors

Morsy Abou SEKKINA[1], Abdul Raouf TAWFIK[1], Osama HEMEDA[1], Mohamad Ahmad Taher DAWOUD[2] and Samy EL-ATTAR[1]
[1]*Faculty of Science, Tanta University, Tanta-EGYPT*
[2]*Faculty of Electronic Engineering El-Menoufia University, Menouf-EGYPT*
e-mail: mohamad_dawoud@maktoob.com

Received 30.03.2004

Abstract

Samples of the nominal composition ($Y_{0.5}Nd_{0.5-x}Ho_x$) $Ba_2Cu_3O_{7-\delta}$, $0 \leq x \leq 0.5$, have been prepared using the conventional solid state reaction. The effect of holmium and neodymium substitution on electrical resistivity, transition temperature T_c, lattice parameters, size of crystallite and grain size has been investigated. X-ray diffraction, electron micro-probe, scanning electron microscope and IR spectra, have been used in our investigation. The results show that the transition temperature T_c, electron-hole jump rate and lattice parameters (a, b) have minimum values at $x = 0.2$, while c increases to maximum at $x = 0.2$. The size of crystallite, the electrical resistivity and grain size are also maximum at $x = 0.2$. The real composition, molecular state and electronic state of the prepared samples are discussed.

Key Words: Superconductors; X-ray; IR-spectra; YBCO; Ho; Nd.

PACS Classification code: 61.10.Nz ; 74.62.Dh ; 74.72.Bk ; 78.30.-j ; 84.37.+q

1. Introduction

The High-T_c superconducting phase in the YBCO system possesses orthorhombic-layered structures [1]. The structure is based on the oxygen deficient tri-perovskite model with the general formula $Y_1Ba_2Cu_3O_6$ with the O(4) sites vacant. Upon oxidizing the material, the added oxygen atoms situate themselves in the O(4) sites, at first filling up alternate Cu-O chains, later occupying and completely filling up the alternate $Y_1Ba_2Cu_3O_{7-\delta}$ oxidized states. Upon further oxidation, the other chains start filling up, and in the fully oxidized state, i.e. $Y_1Ba_2Cu_3O_7$, the O(4) chains are filled up and the 90 K superconducting phase is established. In the high-T_c granular superconductors, transport properties are mainly controlled by the grain boundary microstructure, unlike the T_c which is determined by the crystal structure and oxygen content. Depending on crystallography and structure of boundaries, they can be favorable for the passage of super current or can be weak links (reduced T_c regions) in the superconducting current path of ceramic samples. Recently, many studies have been directed to investigate the dissipation at a separate boundary of different type [2]. Polycrystalline samples of the superconducting oxides ($Y_{1-x}Nd_x$) $Ba_2Cu_3O_{7-\delta}$ were prepared by De Angelis et al. [3]; a scanning electron microscopic investigation indicated 20 micron particle

size in the interior for Nd-containing samples. They also studied energy dispersion X-ray spectroscopy and X-ray diffraction. Micnas et al. [4] studied the type of vibration modes for YBCO and doped YBCO using IR absorption spectra.

The aim of the present work is to study the effect of replacing Nd ions by smaller ionic size Ho ions on the electrical resistivity, diffusion coefficient, lattice parameters, crystallite size, and jump rate of electron-hole in the system $(Y,\ Nd)\ Ba_2Cu_3O_{7-\delta}$. We also, for the first time, correlate these parameters with the transition temperatures.

2. Experimental Work

The prepared samples with the nominal composition $(Y_{0.5}Nd_{0.5-x}Ho_x)\ Ba_2Cu_3O_{7-\delta}$, $0.0 \leq x \leq 0.5$ were prepared by a solid state reaction technique [3, 5, 6] with starting materials Y_2O_3 (99.9%), Nd_2O_3 (99.99%), $BaCO_3$ (99.9%) and CuO (99%). The powders were mixed well in an agate mortar for several hours, as the uniformity and homogeneity of particle size are important for some applications of this superconductor [7]. The mixtures were calcined at 870 °C under O_2 stream for 40 hours, then crushed again and pressed under a pressure of 10 ton/cm^2 into pellets 2 mm thick and 13 mm diameter. Sintering was carried out under O_2 stream at 950 °C [8] for 74 hours. The temperature was slowly cooled down (5 °C/min) to 550 °C and left at this temperature for 36 hours under compressed O_2 stream. The furnace was then switched off and left to cool to room temperature with the samples inside. A levitation test was carried out to check the bulk superconductivity of the samples.

The DC electrical resistivity of the prepared samples was measured as a function of temperature using the modified four-probe technique in a closed cycle refrigerator (EBARA); the current used was $I = 3$ mA. The room temperature X-ray diffraction patterns of the prepared samples were carried out using a Shimadzu- X-ray diffractometer with Cu–Kα ($\lambda = 1.5418$ Å) radiation and nickel-filter. Electron microprobe (EMP) investigations of the samples were carried out on two different regions. The scanning electron microscopic (SEM) investigations of the prepared samples were carried out on fresh fractured surface. To study the morphology of the samples at magnifications 5000×, the surface of samples was finely coated with gold by the use of jeol JFC-1100E ion sputering device. The samples were then placed in a cavity of Jeol JSM-5300 scanning electron microscope under low pressure. Solid KBr infrared absorption (IR) spectra for the prepared samples were carried out at room temperature using Perkin-Elmer-1430 Recording Infrared Spectrophotometer in the range from 200 cm^{-1} to 3000 cm^{-1}. The force constant of the vibration modes was estimated by the following equation [9].

$$f = 4\pi^2 c^2 \upsilon^2 \mu \tag{1}$$

where c is the velocity of light, *upsilon* is the wave number and μ is the reduced mass.

3. Results and Discussion

Figure 1 shows the temperature dependence of DC electrical resistivity for the prepared samples. It is observed that all compounds are metallic in the normal state. The superconductivity is caused by the electron-phonon interaction [10]. The metallic behavior is attributed to the generation of cuprous oxide during sintering, according to the equation

$$2Cu^{2+} \rightarrow Cu^{+} + Cu^{3+} \tag{2}$$

The existence of metallic behavior in our compositions is due to the exchange of electrons between Cu^{2+} and Cu^{3+}, according to the relation:

$$Cu^{2+} \leftrightarrow Cu^{3+} + e$$

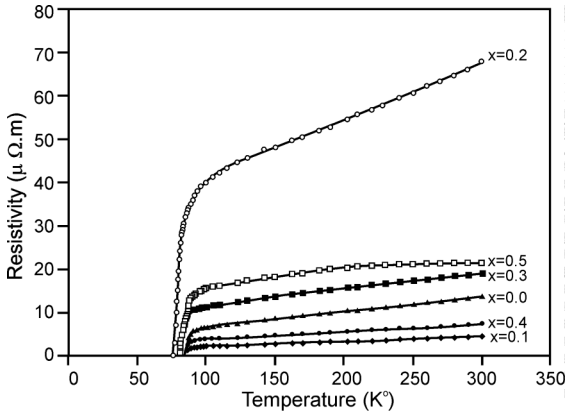

Figure 1. The dependence of Electrical resistivity on holmium content x in the composition $(Y_{0.5}Nd_{0.5-x}Ho_x)$ $Ba_2Cu_3O_{7-\delta}$, $0.0 \leq x \leq 0.5$.

Figure 2 shows that T_c values (onsets and offsets) are found to decrease with increasing holmium concentration and reaches minimum at $x = 0.2$, but for $x > 0.2$ the transition temperature T_c increases.

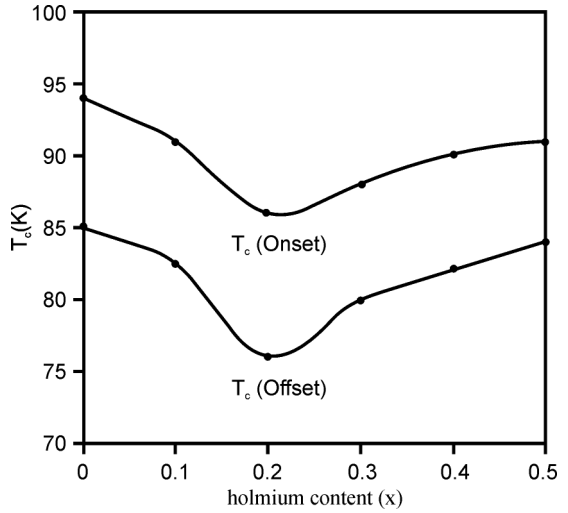

Figure 2. Dependence of T_c offset and T_c onset on holmium content x in the composition $(Y_{0.5}Nd_{0.5-x}Ho_x)$ $Ba_2Cu_3O_{7-\delta}$, $0.0 \leq x \leq 0.5$.

The activation energy ΔE for conduction rises to maximum value at $x = 0.2$, as shown in Figure 3. Thus, the metallic activation energy of the prepared samples is in agreement with their normal state electrical resistivity.

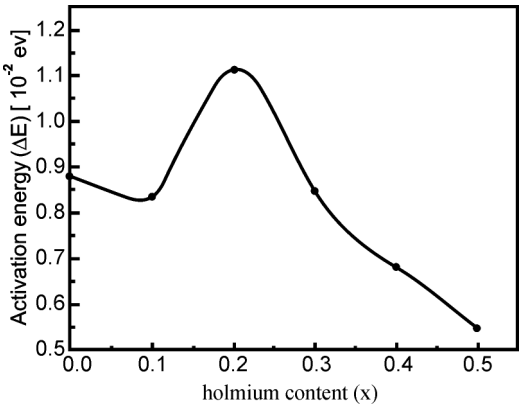

Figure 3. Dependence of the activation energy ΔE on holmium content x in the composition $(Y_{0.5}Nd_{0.5-x}Ho_x)$ $Ba_2Cu_3O_{7-\delta}$, $0.0 \leq x \leq 0.5$.

Figure 4 shows the effect of holmium concentration on the electrical resistivity at 130 and 300 K. It is clear that a pronounced increase in the value of electrical resistivity takes place at $x = 0.2$ and then decreases for $x > 0.2$. Doping is another mechanism for introducing lattice vacancies [11, 12]. For $x \leq 0.2$, the increase in the electrical resistivity can be explained on the basis that the substitution of neodymium ions (r = 0.98 Å) by smaller size holmium ions (r = 0.87 Å) creates lattice vacancies. These generated vacancies act as barrier energy and may capture the electron-hole leading to a decrease of the mobility of electron-hole for conduction throughout the crystal lattice, which increases electrical resistivity with increasing Ho concentration. For $x > 0.2$ the decrease of electrical resistivity with increasing Ho concentration is attributed to the filling of neodymium cation vacancies with the extra holmium ions. The decrease of these vacancies encourages the electron-hole mobility leading to a decrease of electrical resistivity.

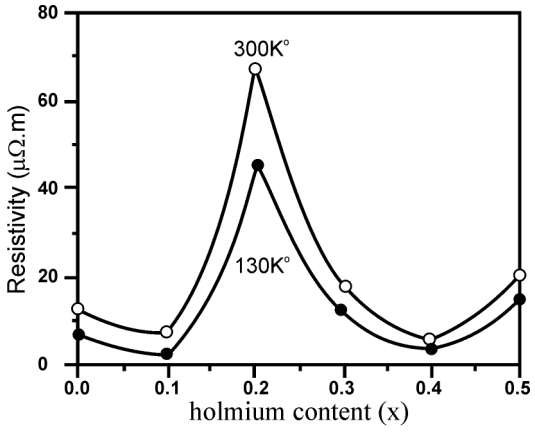

Figure 4. Dependence of Electrical resistivity on holmium content x in the composition $(Y_{0.5}Nd_{0.5-x}Ho_x)$ $Ba_2Cu_3O_{7-\delta}$, $0.0 \leq x \leq 0.5$.

Figure 5, shows the effect of holmium concentration on the electron-hole diffusion coefficient D at room temperature. The diffusion coefficient of electron-hole was estimated by the equation [13],

$$D = \frac{\sigma KT}{N_o e^2}, \tag{3}$$

where $N_0 = 2 \times 10^{28}$ m^{-3} and σ is the electrical conductivity. It is observed that the diffusion coefficient decreases with increasing holmium ions and reaches minimum at $x = 0.2$. For $x > 0.2$ the electron-hole diffusion coefficient increases with increasing x. This may be explained as follows.

Electron-hole diffusion usually takes place via the motion of point defects and is therefore connected thermodynamically with defects. All of the superconducting oxides are nonstoicheiometric compounds [14] whose deviation from stoicheiometry is controlled by the defect equilibria. The defects include the oxygen and cation vacancies in addition to electron-hole defects. These defects affect the Onset T_c of superconductivity. When Ho^{3+} ions substitute Nd^{3+} ions, mechanical pressure is induced producing lattice vacancies, these vacancies inhibit the acceleration of electron-hole generation up to $x = 0.2$ leading to a decrease of electronic diffusion. Above this concentration, the lattice vacancies decrease, enhancing the mobility of electron-hole, leading to an increase of electronic diffusion.

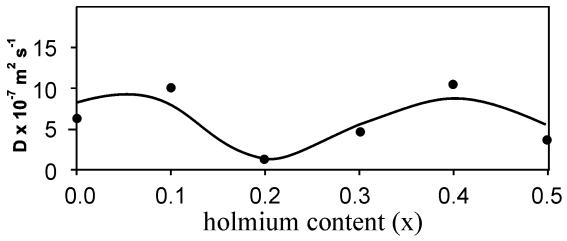

Figure 5. Dependence of diffusion coefficient D on holmium content x in the composition $(Y_{0.5}Nd_{0.5-x}Ho_x)$ $Ba_2Cu_3O_{7-\delta}$, $0.0 \leq x \leq 0.5$.

Figure 6. shows the effect of holmimn concentration on the electron-hole jump rate P at room temperature in the directions of lattice parameters of this orthorhombic superconductors. The jump rate of electron-hole is estimated by using the equations [13]

$$\begin{aligned} D &= a^2 p \\ D &= b^2 p \\ D &= c^2 p \end{aligned} \tag{4}$$

where D is the diffusion coefficient of electron-hole in the direction of applied field and (a, b, c) are the lattice parameters. In this respect the decrease of the electron-hole jump rate for $x < 0.2$ is explained based on the replacement of Y^{3+} by Ho^{3+} ions, the introduction of Ho^{3+} in the crystal lattice induces lattice vacancies [11, 12]. The increase of holmium concentration increases lattice vacancies, which trap the conduction electron-hole. The number of lattice vacancies reaches optimum value at $x = 0.2$ leading to a decrease of electron-hole jump rate. For $x > 0.2$, Ho^{3+} ions of smaller size partially fill Nd^{3+} vacancies, leading to a reduction of lattice vacancies, which increases the mobility of electron-hole and causes an increase of electron-hole jump rate.

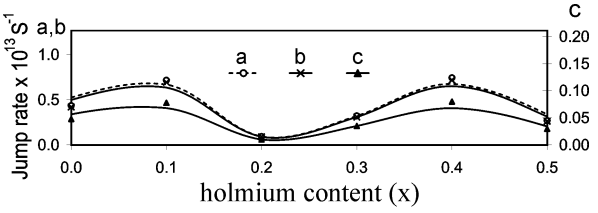

Figure 6. Dependence of jump rate (P) on holmium content x in the composition $(Y_{0.5}Nd_{0.5-x}Ho_x)$ $Ba_2Cu_3O_{7-\delta}$, $0.0 \leq x \leq 0.5$.

Figure 7 shows the X-ray diffraction patterns for the prepared samples. It is clear that our samples belong to the orthorhombic phase at room temperature.

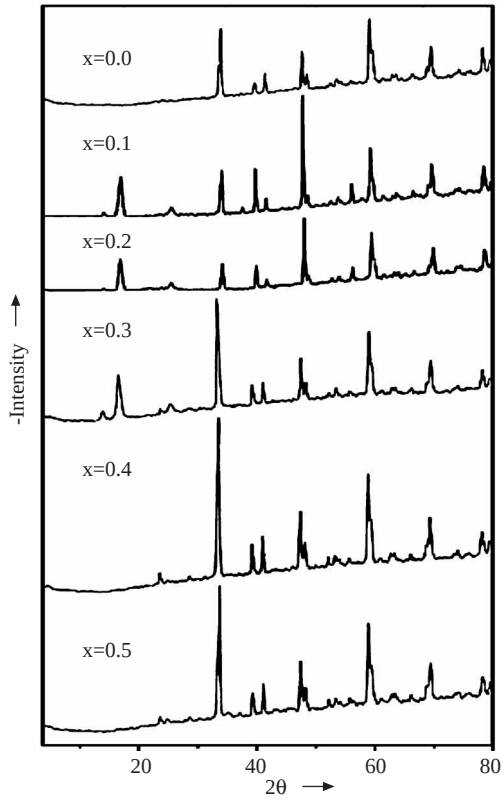

Figure 7. X-ray diffraction patterns for the composition $(Y_{0.5}Nd_{0.5-x}Ho_x)\ Ba_2Cu_3O_{7-\delta}$, $0.0 \leq x \leq 0.5$.

The lattice parameter values (a, b, c) are in agreement with those published for undoped YBCO [15, 16] and doped YBCO [13, 17]. The lattice parameters (a, b) of the prepared samples decrease to minimum value with increasing holmium concentration up to $x = 0.2$ and increase for $x > 0.2$, while lattice parameter c rises to maximum value at $x = 0.2$ and decreases for $x > 0.2$ as shown in Figure 8.

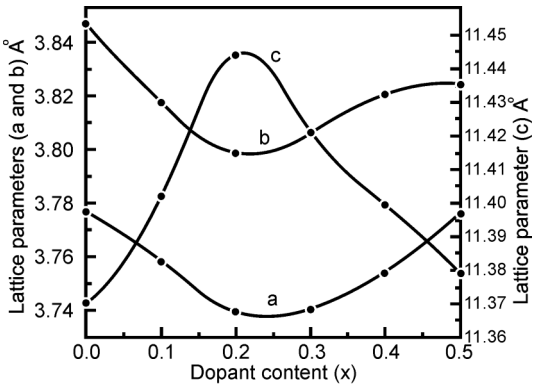

Figure 8. Dependence of lattice parameters (a, b, c) on holmium content x in the composition $(Y_{0.5}Nd_{0.5-x}Ho_x)$ $Ba_2Cu_3O_{7-\delta}$, $0.0 \leq x \leq 0.5$.

As a general trend, there is considerable peak shift towards short interplanar spacing with Ho doping [16]. This is due to the relatively smaller ionic size Ho replacing the larger ionic size Nd. Moreover, an

increased degree of crystallinity at definite Ho concentration for $x = 0.1$ and 0.2, was noticed plus a change in the relative peak intensity (see Figure 7).

The decrease of lattice parameters (a, b) with increasing holmium concentration up to $x = 0.2$ may be due to the difference in radii between Ho^{3+} and Nd^{3+} which results in a shrinkage of the perovskite layer in the structure. Thus, the increased lattice parameters (a, b) beyond $x = 0.2$ will be due to the decrease in hole concentration in the CuO_2 planes [18]. Accordingly, holmium substitution for neodymium would lead to an increase of oxygen vacancies, which is indicated by the decrease of c-axis [19]; these results correlate with the decrease of transition temperature T_c [20]. For the structure $RBa_2Cu_3O_{7-\delta}$, it has been established that Cu(2)-Cu(2) distance across Ba decreases and that of Cu(2)-Cu(2) across the rare earth R increases with ionic radius [21].

For the effect of Ho^{3+} concentration on crystallite size, the average size of the crystallites t was estimated from XRD pattern using Scherrer's equation

$$t = \frac{K\lambda}{h_{1/2}Cos\theta}, \tag{5}$$

where K is Scherrer constant (0.9×57.3), λ is the wavelength of radiation, $h_{1/2}$ is the full width at half maximum in radians and θ is the corresponding angle of the peak position; this is shown in Figure 9.

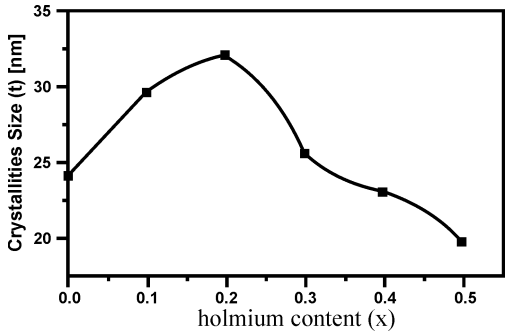

Figure 9. Dependence of crystallites size t at 300 K on holmium content x in the composition $(Y_{0.5}Nd_{0.5-x}Ho_x)$ $Ba_2Cu_3O_{7-\delta}$, $0.0 \leq x \leq 0.5$.

It is observed that the crystallite size of the sample surface increases with increasing holmium concentration to maximum value at $x = 0.2$. For $x > 0.2$, the crystallite size decreases with increasing x value. This can be explained as follows. Doping with Ho^{3+} does not effectively impede crystallite growth, implying that the dopant ions are associated with the charged vacancies they create, and these vacancies are responsible for the attraction between the defects and crystallite boundaries. Thus, the introduction of Ho^{3+}ions is believed to associate uncharged oxygen vacancies because Nd^{3+} ions and Ho^{3+} ions are equal in valency. Furthermore, the defects that are not strongly attracted to the boundaries cannot reduce their mobility, leading to the increase of crystallite growth and domain wall area. This boundary captures the cation vacancies (pores) enhancing the electrical resistivity to maximum value at $x = 0.2$. For $x < 0.2$, the substitution of Nd^{3+} ions by Ho^{3+} ions increases the defect concentration at grain boundaries, acting as a sink for the diffusion of vacancies from pores to grain boundaries. The adsorbed defect might repel vacancies sufficiently for diffusion of grain boundary to become the dominant densification (sintering) mechanism and thus causing the reduction of pores. This, of course, enhances the electrical conductivity. Our results of crystallite size agrees with that cited in previous work [13].

The grain size of the prepared samples was examined using SEM. Figures 10–15 show SEM photographs of the prepared samples.

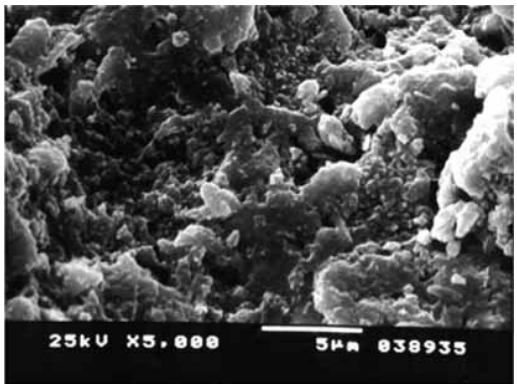

Figure 10. The scanning electron microscopy (SEM) of sample $(Y_{0.5}Nd_{0.5})\ Ba_2Cu_3O_{7-\delta}$.

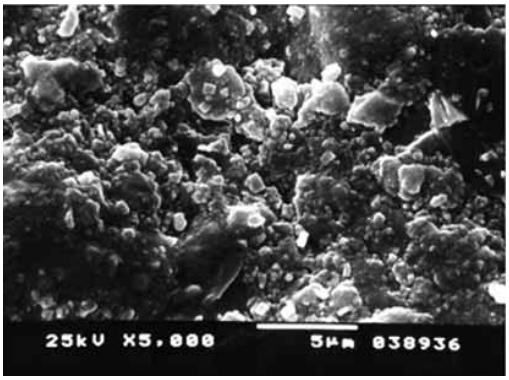

Figure 11. The scanning electron microscopy (SEM) of sample $(Y_{0.5}Nd_{0.4}Ho_{0.1})\ Ba_2Cu_3O_{7-\delta}$.

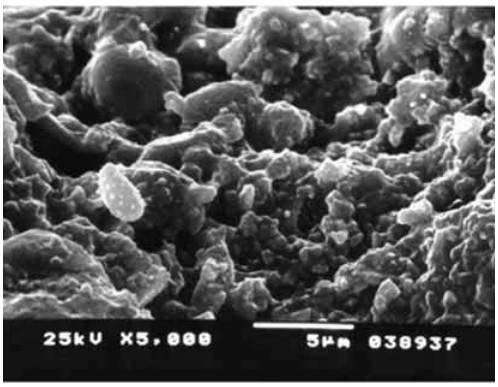

Figure 12. The scanning electron microscopy (SEM) of sample $(Y_{0.5}Nd_{0.3}Ho_{0.2})\ Ba_2Cu_3O_{7-\delta}$.

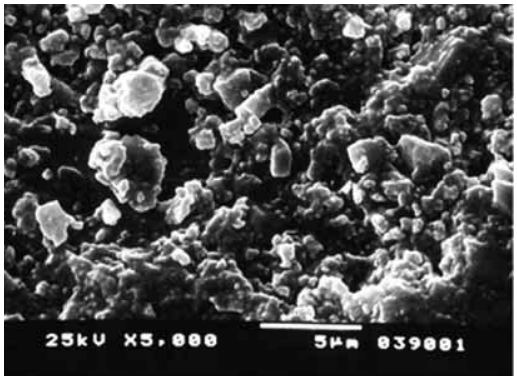

Figure 13. The scanning electron microscopy (SEM) of sample $(Y_{0.5}Nd_{0.2}Ho_{0.3})\ Ba_2Cu_3O_{7-\delta}$.

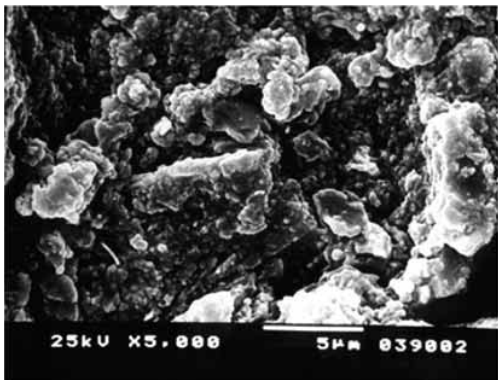

Figure 14. The scanning electron microscopy (SEM) of sample $(Y_{0.5}Nd_{0.1}Ho_{0.4})\ Ba_2Cu_3O_{7-\delta}$.

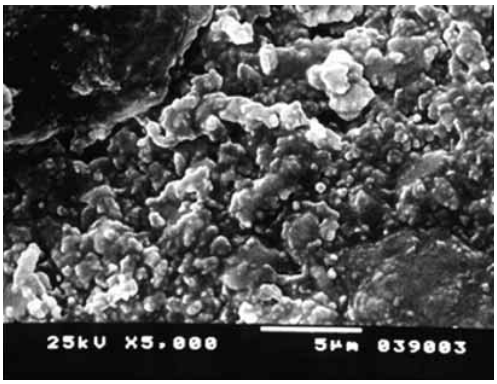

Figure 15. The scanning electron microscopy (SEM) of sample $(Y_{0.5}Ho_{0.5})\ Ba_2Cu_3O_{7-\delta}$.

The rate of grain growth is enhanced with holmium concentration up to $x = 0.2$. Beyond this concentration, the grain growth is inhibited, as illustrated in Figure 16.

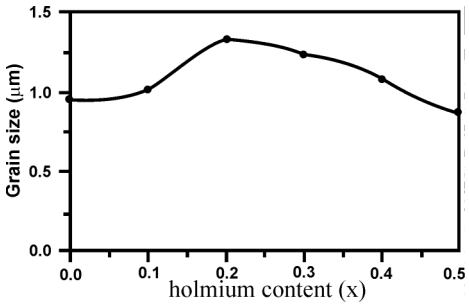

Figure 16. Dependence of grain size at 300 K on holmium content x in the composition $(Y_{0.5}Nd_{0.5-x}Ho_x)$ $Ba_2Cu_3O_{7-\delta}$, $0.0 \leq x \leq 0.5$.

It is believed that the dopant ions concentrate near the grain boundaries which substantially reduce their mobility, and when the boundary moves, adsorbs the impurities. In general, doping does not effectively impede grain growth, implying that the dopant ions are associated with the charged vacancies they create, and these vacancies are responsible for the attraction between the defects and grain boundaries. In our case, Ho^{3+} ions have the same valency as Nd^{3+}, therefore for $x \leq 0.2$ Ho^{3+} ions are not associated with charged vacancies, leading to an increase of grain size. For $x > 0.2$, the increase of Ho^{3+} concentration (which has a smaller radius than Nd^{3+}) encourages these ions to migrate through lattice vacancies during sintering process, which inhibits grain growth.

The infrared absorption spectra of the prepared samples are a rapid tool to determine the electron-phonon interaction and the active fundamental IR modes, give information about the molecular state of the material. Many different groups have worked on infrared vibration spectroscopy of recently discovered HTC-superconducting samples [22–30]. The room temperature IR spectra of the prepared samples are shown in Figure 17.

The spectra are recorded from 200 cm^{-1} to 3000 cm^{-1}; the range from 200 cm^{-1} to 1500 cm^{-1} is usually assigned to the vibration of the crystal lattice [26]. The absorption in this range was observed for pure KBr, and regarded as background for the present experiment. The spectra of the prepared samples have similar trend in the character as that of the standard YBCO [32], which indicates a general feature in common of these related group of our ceramic superconductors. The most important features of these IR spectra are:

a) In the IR spectra of our double-doped YBCO, there are no characteristic bands at 692 cm^{-1} for $BaCuO_2$ and at 482 cm^{-1} and 528 cm^{-1} for $Y_2Cu_2O_5$, which confirms that the prepared samples generally belong to the orthorhombic phase.

b) Adopting the generally accepted notation [4, 32], the type of vibrations $\upsilon_1, \upsilon_2, \upsilon_3$ and υ_4 found for perovskite superconductors are as follows:

υ_1: IR bands in the range from 450 cm^{-1} to about 700 cm^{-1} are due to Cu-O vibration stretching in the oxygen copper polyhedra, with force constant $f = 2.5 \times 10^5$ to 2.757×10^5 dyne/cm^2.

υ_2: The band with maximum at ≈460 cm^{-1} is ascribed to bending vibration of O-Cu-O.

υ_3: The bands below 200 cm^{-1} are ascribed to deformation vibrations of oxygen-copper polyhedra with simultaneous cation displacement and significant contribution of deformation vibration modes of yttrium or rare-earth polyhedra.

υ_4: The bands within the range 250–400 cm^{-1} are ascribed to bending vibration of Cu-O and R-O, R= rare-earth.

The lowest energy vibration is of course related to lattice vibrations of the materials themselves. The spectra of our samples are associated with harmonic vibration. We should point out that in the entire spectra region studied, we observed broad bands that could indicate overlapping of some electronic bands and their hybridization. Values of the force constant for stretching and deformation modes decrease and reach minimum values at $x = 0.2$, and then they increase with increasing Ho^{3+} content x; this behavior is

related to the lattice structure of the unit cell. The force constant is related to the bond length, which is affected, by the ion population, vacancy concentration, and lattice parameters, for the same sample with $x = 0.2$, the lattice parameters (a, b) are minimum, which decrease bond length and make the force constant to be minimum at this value. For $x > 0.2$, the force constant increases with increasing holmium content. From micro structure analysis, the grain size is maximum at $x = 0.2$ and decreases above this value leading to an increase of bond length; consequently, the bond vibration increases and the force constant increases.

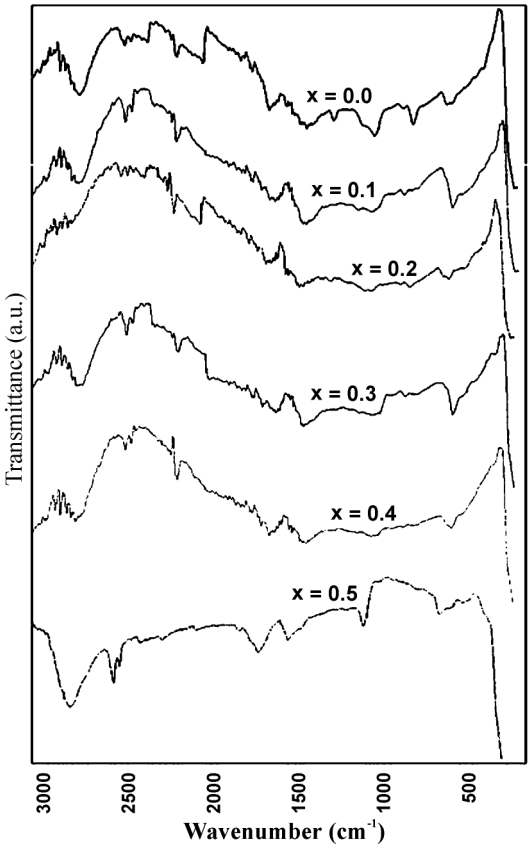

Figure 17. The obtained room temperature infrared absorption spectra of the composition $(Y_{0.5}Nd_{0.5-x}Ho_x)$ $Ba_2Cu_3O_{7-\delta}$, $0.0 \leq x \leq 0.5$.

The intensity of the absorption bands for stretching mode has the same behavior as the force constant, and this may be attributed to population of ions and lattice vacancies. At $x = 0.2$ lattice vacancies are maximum and the population is minimum which results in a lower absorption intensity; the intensity of deformation mode of vibration reaches maximum at $x = 0.2$. The lattice vacancies are maximum at this value of holmium content, then the lattice deformation increases, followed by an increase of lattice vibration intensity. This will lead to an increase of electrical resistivity. In conclusion, the dopant cations cause some perturbation in (Cu-O) and (rare earth-O) bond length, which affects the bond vibration frequency and bond intensity.

4. Conclusion

We can conclude that all samples with the composition $(Y_{0.5}Nd_{0.5-x}Ho_x)$ $Ba_2Cu_3O_{7-\delta}$, $0.0 \leq x \leq 0.5$, are metallic in the normal state and superconducting at lower temperatures, but a critical value of $x = 0.2$ is observed.

Below this concentration, electrical resistivity, activation energy, crystallite size, lattice parameter c and average grain size increase, while the critical temperature, the diffusion coefficient, lattice parameters (a, b) and jump rate decrease. This may be attributed to the creation of lattice vacancies leading to capturing the electrons.

Above that concentration, the extra Ho ions fill the Nd vacancies leading to a decrease of lattice vacancies and an increase of electrons. That may explain the changeover of the previous parameters.

The critical concentration $x = 0.2$ is explained in view of what it may be a migration of Y ions to interstitial sites.

References

[1] Z. G. Fas, C. L. Ji and J. T. Wun, *Mod. Phys. Lett, B,* **3**, (1989), 1009.

[2] S. E. Babcock and J. L. Vargas, *Annu. Rev. Mater. Sci.*, **25**, (1995), 193.

[3] R. J. De Angelis, J. W. Brill, M. Chung, W. D. Arnett, X. D. Xiang, G. Minton, L. A. Rice and C. E. Hamrin: *Solid State Comm.*, **64**, (1987), 1353.

[4] R. Micnas, I. Onyszkiewicz and P. Czarnecki; *Physica B*, **147**, (1987), 166.

[5] J. W. Lynn, High Temperature Superconductivity, New York, (1990).

[6] E. Kandyel, X. J. Wu and S- Tajima, *J. of Physics and Chemistry of Solids*, **61**, (2000), 1379.

[7] H. Kuepler, I. Apfelstedt, W. Schauer, R. Fluekiger, R. Meier- Hirmer and H. Wuehl, *Z-Phys. B,* **69**, (1987) 159.

[8] S. Ozcan, T. Firat and E. Ozdas; *Turk. J. Phys.*, **26**, (2002), 435 .

[9] O. M. Hemeda, M. Z. Said and M. M. Barakat; *Journal of Magnetism and Magnetic Materials*, **224**, (2001), 132.

[10] B. N . Onwuajba, *Turk. J. Phys.*, **26**, (2002), 403.

[11] R. B. Atkin, R. B. Holman and R. M. Fulrath, *J. Amer, Ceram. Soc.*, **54**, (1971), 113.

[12] R. B. Atkin and R. M. Fulrath, *J. Amer. Ceram. Soc.*, **54**, (1971), 265.

[13] A. E. Hughes and D. Pooley, Real Solids and Radiation, Wykeham Publication (London), (1975), 62.

[14] J. L. Routort and S. J. Rothman, *J. Appl. Phys.*, **76**, (1994), 5615.

[15] J. M. Tarascon, P. Barboux, P. F. Miceli, L. H. Green, and G. W. Hull; *The Amer. Physical Society*, **37**, (1988), 7458 .

[16] K. B. Garg, S. M. Bose; High Temperature Superconductivity, Naroso Publishing House, India, (1998), 293.

[17] Kh. M. Elsabawy; M .Sc . Thesis, Tanta University, Tanta, Egypt, (1997).

[18] O. Chmaissem, L. Wessels and Z. Z. Sheng, *Physica C*, **230**, (1994), 231.

[19] X. F. Sun, X. Zhoa, L. Wang, Q. F. Zhou, W. B. Wu and X. G. Li, *Physica C*, **324**, (1999), 193.

[20] Y. Zhao, H. Zhang, S. F. Sun, Z. Y. Chen; *Physica C*, **15**, (1988), 513.

[21] Y. Le. Page, T. Siegrist, S. A. Sunshina, L. F. Schneemeyer. D. W. Murphy, S. M. Zahurak, J. V. Waszczak, W. R. Mckinnon, J. M. Tarascon, G. W. Hull and L. H. Greene; *Phys. Rev. B*, **36**, (1987), 3617.

[22] N. Ogita, K. Ohbayashi, M. Udagawa, Y. Aoki, Y. Maeno and T. Fujita; *Jpn. J. Appl. Phys.,* **26**, (1987), 415.

[23] K. K. Singh, P. Gungly and J. B. Goodenough: *J. Solid State Chem.*, **52**, (1984), 254.

[24] K. Ohbayashi, N. Oigita, M. Udagawa, Y. Aoki, Y. Maeno and T. Fujita. *Jpn. J. Appl. Phys.*, **26**, (1987), 420.

[25] N. Ogita, M. Udagawa and K. Ohboashi: *Jpn. J. Appl. Phys.*, **26**, (1987), 1005.

[26] G. Ruani, C. Taliani, R. Zamboni, D. Cittone and F. C. Matacotta: *J. Opt. Soc. Am. B*, **6**, (1989), 409.

[27] C. Jianmin, X. Leimin, Z. Yonggang, C. Peixin and G. Huifang: *Physica C*, **159**, (1989), 317.

[28] Y. Hong-Juany, Y. Zhi-Yi, L. Wei, J. Hua-Mei, C. Jian-Xiang, L. Guang-Yuan, C.Pei-Xin and G. Wei-Fang: *Acta Phys. Sin.*, **38**, (1989), 586.

[29] A. J. Pal, P. Mandal, A. Podder and B. Ghosh; *Physica C*, **181**, (1991), 186.

[30] C. H. Ruscher, M. Gotte, B. Schmidt, C. Quitmann and G. Guntherodt; *Physica C*, **204**, (1992), 30.

[31] S. A. Mazen, F. Metawe, S. F. Mansour;*J. Phys. D*, (1997), 30.

[32] R. Grinter, M. J. Harding and S. F. Mason, *J. Chem. Soc.*, **A11**, (1970), 670.